Journal of Applied Physics

RESEARCH ARTICLE | DECEMBER 16 2024

Phase transitions in the Co-doped Heusler alloy $Ni_2Mn_{1-x}Co_xGa$

Special Collection: Multicalorics II

Jing-Han Chen ; Tej Poudel Chhetri ; Nathaniel Wrobel ; Xiaojian Bai; David P. Young ; Igor Dubenko ; Saikat Talapatra ; Naushad Ali ; Shane Stadler

J. Appl. Phys. 136, 233901 (2024)
https://doi.org/10.1063/5.0226767

Journal of Applied Physics ARTICLE pubs.aip.org/aip/jap

Phase transitions in the Co-doped Heusler alloy $Ni_2Mn_{1-x}Co_xGa$

Cite as: J. Appl. Phys. **136**, 233901 (2024); doi: 10.1063/5.0226767
Submitted: 3 July 2024 · Accepted: 27 November 2024 ·
Published Online: 16 December 2024

Jing-Han Chen,[1,a)] Tej Poudel Chhetri,[1] Nathaniel Wrobel,[1] Xiaojian Bai,[1] David P. Young,[1] Igor Dubenko,[2] Saikat Talapatra,[2] Naushad Ali,[2] and Shane Stadler[1]

AFFILIATIONS

[1]Department of Physics and Astronomy, Louisiana State University, Baton Rouge, Louisiana 70803, USA
[2]School of Physics and Applied Physics, Southern Illinois University, Carbondale, Illinois 62901, USA

Note: This paper is part of the special topic, Multicalorics II.
[a)]**Author to whom correspondence should be addressed:** jhchen10@lsu.edu

ABSTRACT

The phase transitions of a series of Co-doped Heusler alloys, $Ni_2Mn_{1-x}Co_xGa$ ($0 \leqslant x \leqslant 0.2$), were investigated experimentally using the magnetization measurements, x-ray diffraction, and calorimetric measurements up to their respective melting points. With increasing Co concentration, the structural transition temperatures, Curie temperatures, and melting points, were observed to increase, while the order–disorder transition temperatures decreased. Temperature-dependent x-ray diffraction experiments revealed two different crystal structures in the low-temperature martensite phase for different Co concentrations. However, above their respective structural transitions, both low-temperature crystal structures transformed into the $L2_1$ cubic structure. These findings enabled the construction of a complete magnetic and structural phase diagram for $Ni_2Mn_{1-x}Co_xGa$, spanning from cryogenic temperatures to the melting points. The temperature-dependent XRD results revealed the abrupt changes in interatomic Mn–Mn distances, which validates the crucial role of Mn–Mn interatomic distance and the effect of the magnetic coupling competition in the structural stability between the martensite phase and austenite phase.

I. INTRODUCTION

Heusler alloys are ternary intermetallic compounds with the composition X_2YZ. They have been the subject of many investigations since the discovery of the first ferromagnetic copper-manganese-based alloys by Heusler *et al.*, in 1903.[1] Interest in Ni-Mn-Z-based Heusler alloys, with $Z = Ga$,[2–5] In,[5–13] Sb,[5,6,14–19] or Sn,[5,6,18,20] has grown significantly because the alloys with these compositions have magnetic phase transition occurring close to room temperature, which make them potential refrigerants for magnetic cooling and ferromagnetic shape-memory devices operating at room temperature.[21,22]

Among these Heusler alloys, Ni_2MnGa has drawn considerable interest after being discovered in 1960[23] because it exhibits ferromagnetic shape-memory behavior across its martensitic structural transition occurring at ≈ 220 K.[2] Below its structural transition temperature, the martensite phase of Ni_2MnGa is a modulated monoclinic crystal structure with ferromagnetic ordering.[24–27] As the temperature increases above its structural transition temperature, the structure transforms to a ferromagnetic austenite phase with the $L2_1$ cubic structure with Curie temperature of 365 K.[2] As the temperature continues to increase, the ordered atomic arrangement of Mn and Ga of the $L2_1$ cubic structure is entirely destroyed at 800 °C, leading to the formation of a disordered B2 cubic phase.[28,29] Mn and Ga atoms in the $L2_1$ cubic ordered phase occupy two distinct positions, whereas they are randomly distributed in the B2 cubic disordered phase. The structural variation between the martensite phase, ordered $L2_1$ austenite phase, and disordered B2 austenite phase in Ni_2MnGa Heusler alloys is depicted in Fig. 1.

Considering that the Mn atoms in Ni_2MnGa Heusler alloys provide the dominant contribution to the magnetic interactions,[2,31,32] other studies have demonstrated that the magnetic and structural transitions can be concurrently adjusted by replacing some Mn atoms with Fe,[33–35] Co,[36–39] Cr,[40–42] Cu,[3,37,39,43–50] or V[51] atoms. To increase our understanding of the effects of atomic

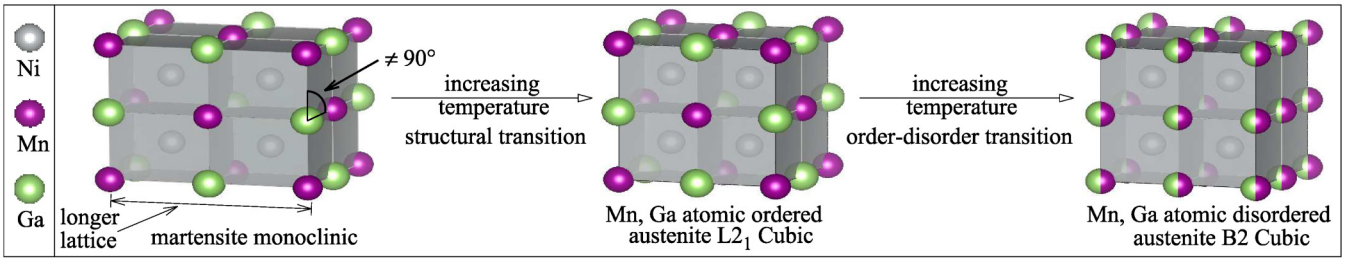

FIG. 1. The structure variation between the martensite phase, ordered austenite phase, and disordered austenite phase in Ni_2MnGa Heusler alloys is illustrated in a polyhedral representation by VESTA.[30] Mn and Ga atoms in the $L2_1$ cubic ordered phase are situated in two distinct positions, whereas Mn and Ga atoms in the B2 cubic disordered phase exhibit a completely random distribution.

substitution on the phase transitions in Ni_2MnGa Heusler alloys, polycrystalline alloys with compositions $Ni_2Mn_{1-x}Co_xGa$ ($0 \leqslant x \leqslant 0.2$) were prepared and a systematic study of their properties through magnetic, calorimetric, and temperature-dependent x-ray diffraction (XRD) measurements was performed. It was observed that, as the Co concentration increases, the structural transition temperatures, Curie temperatures, and melting points increased, whereas the order–disorder transitions decreased. Meanwhile, from temperature-dependent XRD measurements, two different crystal structures in the low-temperature martensite phase were found for different Co concentrations, but all the samples ultimately crystallized in the $L2_1$ cubic structure upon heating above their respective structural transition temperatures. The experimental results were employed to construct a complete magnetic and structural phase diagram as a function of Co concentration, spanning from below their respective structural transition temperatures to their melting points. Abrupt changes in interatomic Mn–Mn interatomic distances derived from the temperature-dependent XRD results were observed, validating the crucial role of Mn–Mn interatomic distance and the effect of the magnetic coupling competition in the structural stability between the martensite phase and austenite phase.

II. SAMPLE PREPARATION

Polycrystalline $Ni_2Mn_{1-x}Co_xGa$ ingots ($x = 0, 0.10, 0.15,$ and0.20) were fabricated from high purity (>99.95%) Ni, Mn, Co, and Ga components by melting in a radio frequency induction furnace under argon atmosphere. The samples are labeled as Co-00 ($x = 0$), Co-10 ($x = 0.10$), Co-15 ($x = 0.15$), and Co-20 ($x = 0.20$). The weight loss after melting was found to be less than 0.3% for each sample. The melted ingots were first heat treated at 1100 °C for 12 h. The heat treated ingots were ground into powders and then annealed at 700 °C for three days before being cooled slowly.

To confirm the compositional homogeneity of the powder samples, composition analysis was carried out using Oxford energy dispersive spectroscopy (EDS) detector installed on a ThermoFisher Helio G5 Xe PFIB/SEM system. Fifteen different spots across the Co-00 powder samples were analyzed, resulting in the measured compositions of $Ni_{2.06\pm0.10}Mn_{1.07\pm0.05}Ga_{0.87\pm0.14}$. Based on these results, we assumed that the compositions of all the powder samples are homogeneous after the grinding and heat treatment processing.

To confirm the crystalline purity for the prepared samples, powder XRD patterns were measured at room temperature using a Scintag XDS2000 powder diffractometer with Cu Kα radiation. The results are shown in Fig. 2. Samples Co-00, Co-10, and Co-15, exhibited $L2_1$ cubic crystal structures while sample Co-20 crystallized in a $D0_{22}$ tetragonal crystal structure. No perceivable secondary crystalline phases were detected in the scans. Their respective magnetic, thermal, and structural properties are summarized in Table I.

III. THERMAL PROPERTIES

To reveal any potential phase transitions in our samples, a simultaneous differential scanning calorimeter (DSC) and

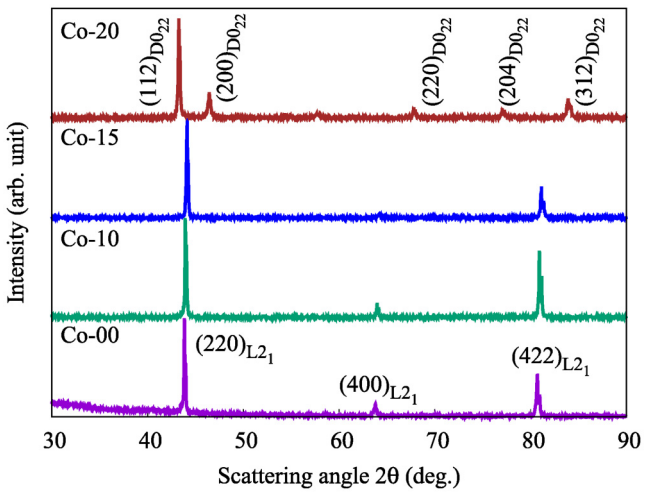

FIG. 2. Room-temperature powder XRD patterns were obtained for all samples. $L2_1$ cubic crystal structures were observed for samples Co-00, Co-10, and Co-15, while a $D0_{22}$ tetragonal crystal structure was found for sample Co-20. The respective Miller indices (in parentheses) of the $L2_1$ cubic and $D0_{22}$ tetragonal crystal structures are shown.

TABLE I. Thermal, structural, and magnetic properties of $Ni_2Mn_{1-x}Co_xGa$ ($0 \leqslant x \leqslant 0.2$) derived from experimental results.

Label	Composition $Ni_2Mn_{1-x}Co_xGa$	T_{Curie}[a] (K)	Structural transition[b]		$T_{L2_1 \leftrightarrow B2}$[c] (°C)	$\frac{\partial V}{\partial T} \times 10^{-3}$[d] (Å^3/K)	M_{sat}/f.u.[e] (μ_B)
Co-00	$x = 0.00$	364.6	213 K	$(mcl. \rightarrow L2_1)$	797	2.11	4.25
Co-10	$x = 0.10$	384.0	244 K	$(D0_{22} \rightarrow L2_1)$	788	2.07	3.89
Co-15	$x = 0.15$	388.1	278 K	$(D0_{22} \rightarrow L2_1)$	785	2.18	3.75
Co-20	$x = 0.20$	397.2	342 K	$(D0_{22} \rightarrow L2_1)$	780	2.09	3.51

[a]Curie temperature estimated by the temperature derivative of the magnetization results shown in Fig. 5.
[b]Structural transition temperature determined by averaging the hysteretic peaks from the temperature derivatives of the magnetization results shown in Fig. 5 and the corresponding crystal structures obtained from the temperature-dependent XRD described in Sec. V.
[c]$L2_1 \leftrightarrow$ B2 order–disorder transition temperature estimated from the temperature derivative of the calorimetric results in Sec. III.
[d]The rate of volume change estimated from temperature-dependent XRD experiments, detailed in Sec. V.
[e]Saturation magnetization estimated from the isothermal magnetization at 2 K as shown in Fig. 6.

thermogravimetric analysis device (model: SDT Q600 manufactured by TA instruments, Inc.) was used. The experiments were performed by heating the samples from room temperature until they melted, and then cooling down to room temperature. The results for sample Co-20 are shown in Fig. 3 as a representative measurement. As the temperature increases from room temperature, the order–disorder transition between $L2_1$ and B2 at 780 °C was first detected, and then the melting/solidification temperature with thermal hysteresis was observed around 1150 °C, as shown in Fig. 3. Similar thermal behaviors were observed in the samples with different Co concentrations. As illustrated in Fig. 4, with increasing Co concentration, the melting points (estimated by averaging the peaks positions from the hysteretic heating and cooling measurement) (solid lines) increased, whereas the order–disorder transitions (dashed lines) decreased. The sample with the highest Co concentration (Co-20) exhibited the lowest order–disorder transition temperature, which was 780 °C. Note that the samples in the current work were annealed at 700 °C for three days before being cooled slowly, and hence atomic order were maximally promoted.

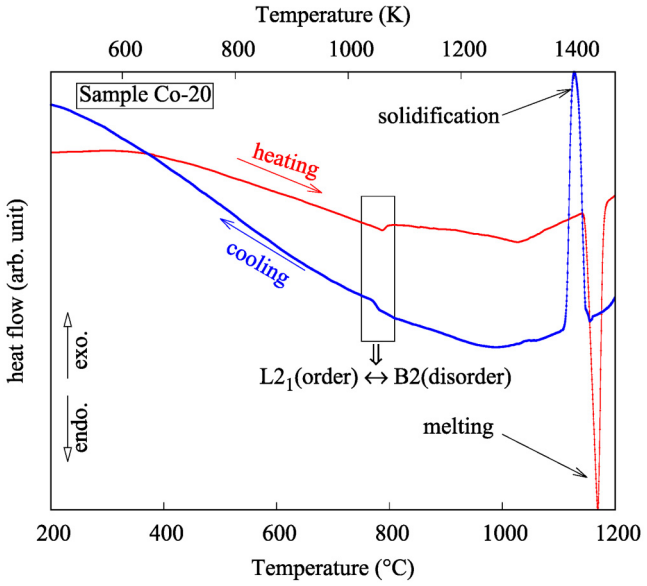

FIG. 3. The heat flow curves for sample Co-20 with temperature sweeping directions indicated by arrows. The transition between ordered $L2_1$ and disordered B2 phases at 780 °C was identified, while the melting/solidification temperature, accompanied by thermal hysteresis, was observed around 1150 °C. Similar thermal behaviors were observed in the samples with different Co concentrations.

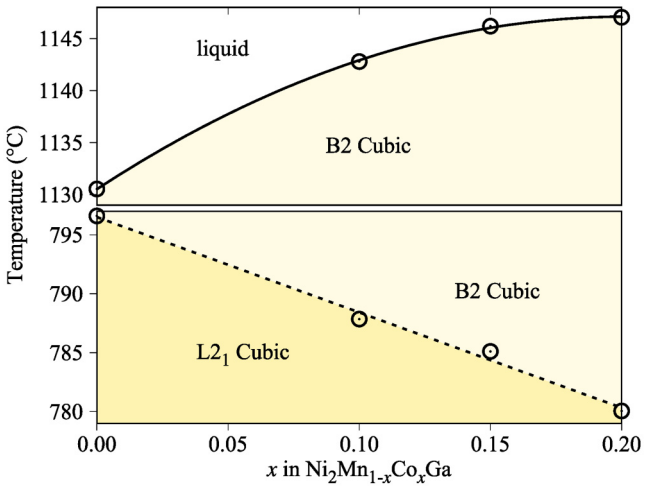

FIG. 4. A phase diagram illustrating the order–disorder transitions and melting points of $Ni_2Mn_{1-x}Co_xGa$ ($0 \leqslant x \leqslant 0.2$) as a function of temperature and Co concentration. With increasing Co concentration, the order–disorder transition temperatures (dashed lines) decreased, while the melting points (solid lines) increased.

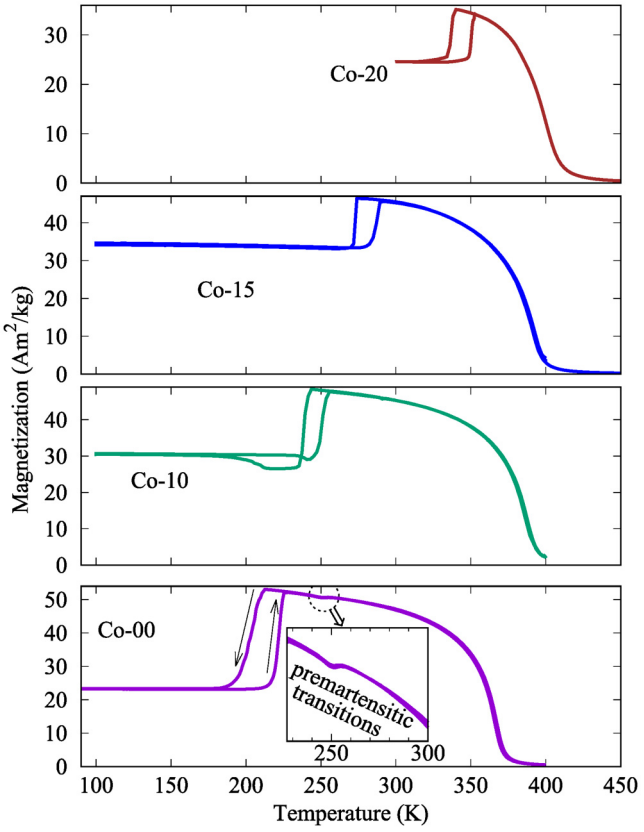

FIG. 5. Temperature-dependent magnetization measurements were conducted on all $Ni_2Mn_{1-x}Co_xGa$ samples using field-cooled cooling and field-cooled warming protocols at $H = 1000$ Oe. The experimental temperature sweeping directions are indicated by arrows in the results of sample Co-00 as a representative curve. The clear thermal hysteresis resulting from first-order structural transitions was observed, with the transition temperatures observed to rise with increasing Co concentration. The bottom inset shows a premartensitic transition as observed from several previously experiments.[52–54]

IV. MAGNETIC PROPERTIES

Magnetization measurements were conducted using a magnetic property measurement system or Dynacool physical property measurement system with the vibrating sample magnetometer oven option manufactured by Quantum Design. Isofield temperature-dependent magnetization measurements were conducted using field-cooled cooling and field-cooled warming protocols at $H = 1000$ Oe, and the results are shown in Fig. 5. For all the samples, a noticeable thermal hysteresis stemming from the first-order structural transitions was found before their Curie temperatures. Both the structural transition and magnetic transition increase with increasing Co concentration. The magnetic and structural transition temperatures obtained from the magnetization experiments are provided in Table I.

The saturation magnetizations of these samples were investigated through isothermal magnetization measurements performed at 2.0 K with fields up to 7 T, as shown in the inset of Fig. 6 (for samples Co-00 and Co-20).

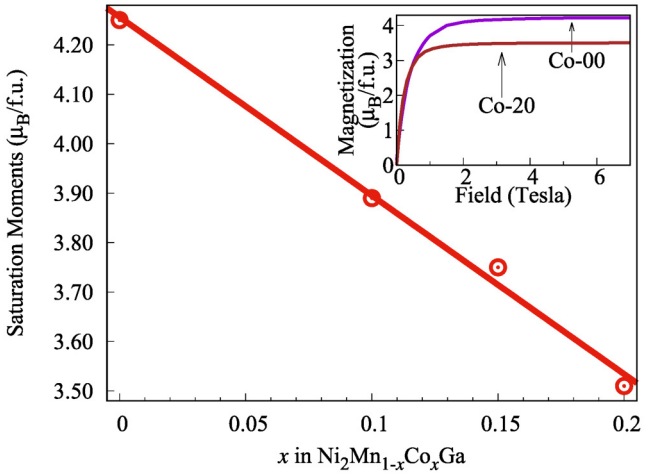

FIG. 6. A linear decrease in saturation moment was found with increasing Co concentration. The inset displays isothermal magnetization results for samples Co-00 and Co-20 at 2.0 K, conducted in fields up to 7 T.

The saturation magnetization (M_{sat}) values were estimated by fitting the experimental magnetization data using the law of approach-to-saturation,

$$M(H) = M_{sat}\left(1 - \frac{a}{H^2} - \frac{b}{H^3}\right),$$

where a and b are fitting parameters.[55,56] The fitted M_{sat} values are provided in Table I. It is found that the saturation moment decreases linearly as the Co concentration increases, similarly as $Ni_2Mn_{1-x}Cu_xGa$.[3,49] As the doping of the smaller atom Co increases in $Ni_2Mn_{1-x}Co_xGa$, the Mn-Mn interatomic distances decrease. As a results, it strengthens the Mn–Mn magnetic exchange interactions and broadens the electronic bands. The former leads to the Curie temperatures increase, while the latter results in the overlap of the atomic states, and hence decreases the magnetic moments.[57–60]

V. STRUCTURAL PROPERTIES

The temperature-dependent x-ray diffraction experiments were performed using a wavelength of 0.457 87 Å at the x-ray Science Division 11-BM beamlines, Advanced Photon Source, Argonne National Laboratory. The structural analyses, including lattice constants and unit cell volumes, were conducted using a general structure analysis system (*GSAS-II*) software.[61] In the following sections, the analysis results of the martensite phase, austenite phase, and structural transition will be presented and discussed.

A. Martensite and austenite phases

Regarding the crystal structures of the martensite phases (below their respective structural transitions), sample Co-00

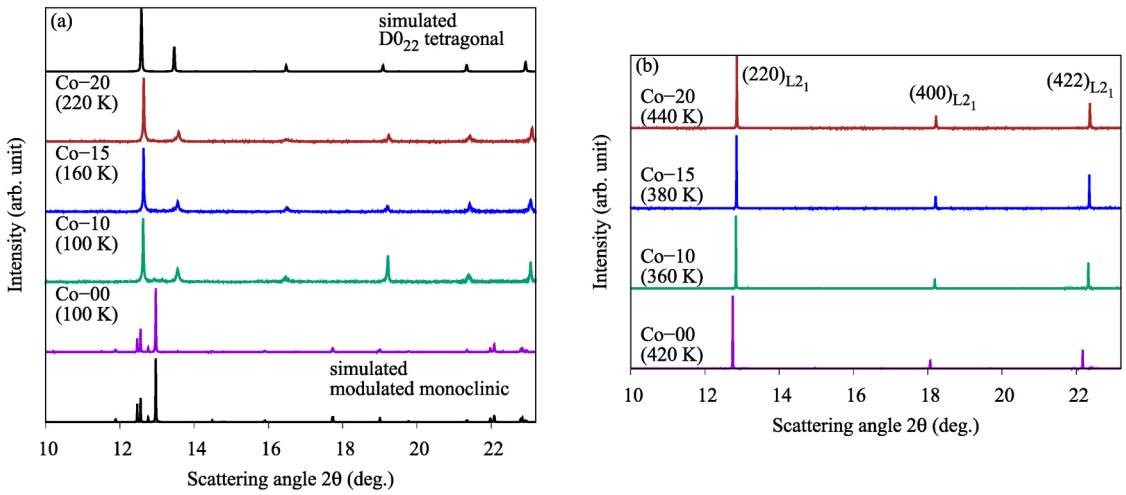

FIG. 7. XRD patterns of samples Co-00, Co-10, Co-15, and Co-20 with the x-ray wavelength 0.457 87 Å. (a) XRD patterns of the martensite phase at the specified temperatures. As a reference, the simulated modulated monoclinic and D0$_{22}$ tetragonal XRD patterns are provided in the bottom and top panels, respectively. (b) XRD patterns of the austenite phase at the specified temperatures. The respective Miller indices (in parentheses) of the L2$_1$ cubic crystal structures are provided.

assumes the XRD pattern of a modulated monoclinic crystal structure with the superspace group $I2/m(\alpha 0\gamma)00$ and modulation vectors $0.433c^*$ ($\approx 3/7c^*$), which is similar to previously reported observations,[24–27,62] while the other samples show the XRD pattern of the D0$_{22}$ tetragonal structure, similar to that reported for $Ni_2Mn_{1-x}Cu_xGa$.[3,63] The XRD results of the martensite phase for all the samples at the indicated temperatures are shown in Fig. 7(a). Although two different crystal structures in the martensite phases were found, the XRD patterns of the austenite phase (above their respective structural transitions) shown in Fig. 7(b) reveal that all the samples crystallize in the L2$_1$ cubic crystal structure.

By incorporating the structural analysis, magnetization, and calorimetric measurements, a comprehensive phase diagram depicting the structural and magnetic information up to the melting points was constructed (Fig. 8). The magnetic and order–disorder transitions shown as dashed lines are second-order phase transitions, while the structural transitions and melting/solidification temperatures shown as solid lines are first-order phase transitions.

B. Structural transitions

To further investigate how the crystal structures evolve across the structural transitions in our samples, XRD experiments at several different temperatures (above and below the structural transitions) were performed. As the doping of Co for Mn was introduced, the austenite phase remained in a L2$_1$ cubic structure and the martensite phase transformed from the monoclinic structure to the tetragonal structure. The volume changes were found to be linear as a function of temperature for all the samples. The rates of the volume change (Å^3/K) on both sides of the structural transition are comparable, as illustrated in Fig. 9. The respective rates are provided in Table I.

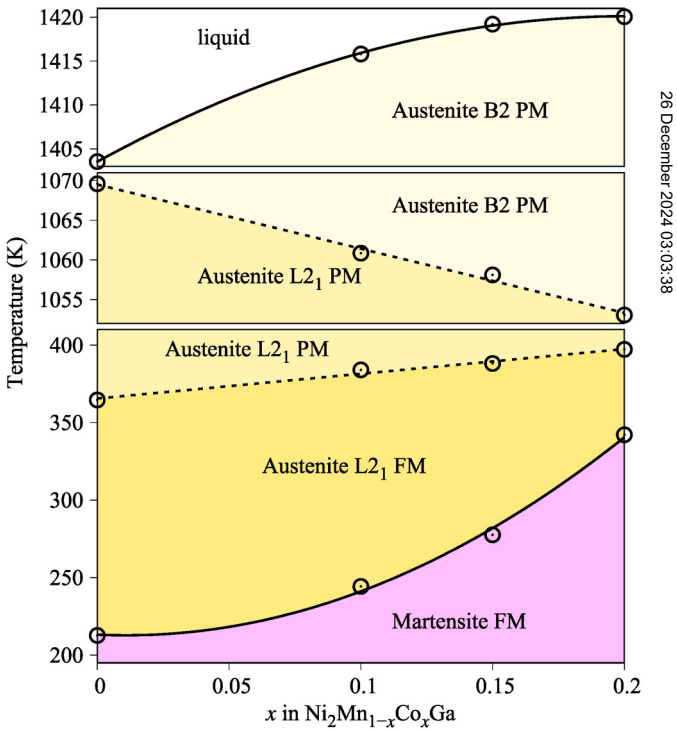

FIG. 8. A complete phase diagram depicting the structural, magnetic, order-disorder transitions, and melting points in $Ni_2Mn_{1-x}Co_xGa$ ($x \leqslant 0.2$) Heusler alloys. The magnetic and order-disorder transitions, characterized as second-order phase transitions, are indicated by dashed lines while the structural transitions and melting points, identified as first-order phase transitions, are shown as solid lines.

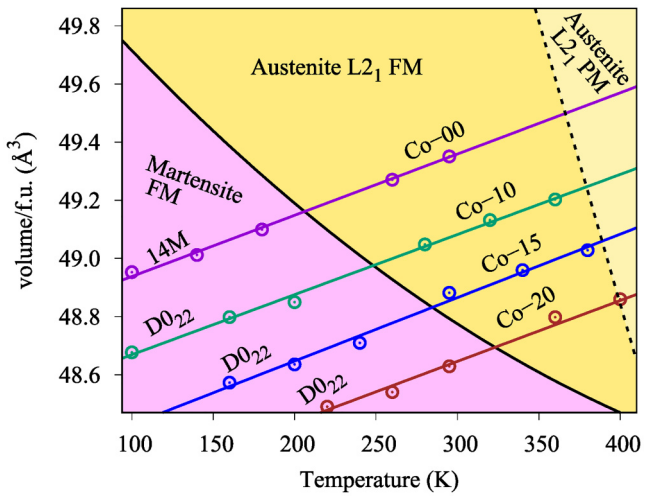

FIG. 9. Variations in cell volumes across the phase transitions were determined from XRD data. Comparable linear changes of volume with temperature were observed on both sides of the structural transitions.

Although there is no abrupt change of the volumes across/between the martensite and austenite phase, it is known that the first-order magnetic transition is subject to a discontinuous change of the magnetic exchange interaction as a function of the distance between magnetic elements.[64,65] In the case of Ni_2MnGa Heusler alloys, we further explore the interatomic Mn–Mn distance because it was found that the structural stability depends critically on the magnetic interactions between Mn atoms.[32] By exploring our temperature-dependent XRD results across the structural transition further, the abrupt discontinuous splitting/changes in the Mn–Mn interatomic bonds was observed, the results of which are presented in Fig. 10.

Considering the highly symmetric austenite $L2_1$ cubic phase, there is only one set of Mn–Mn interatomic bonds, with the coordination number 12, as illustrated on the right side of Fig. 10. The magnetic interaction in this coordination is clearly ferromagnetic. In the martensite phase, either the monoclinic structure with β close to 90° in Co-00 or the tetragonal structures in the other samples was found to stretch further along the c axis than the others.[24,62] During the structural transition, one distinct set of the Mn–Mn interatomic bonds in the austenite $L2_1$ cubic phase is split into two major sets of Mn–Mn interatomic bonds in the low-temperature martensite phase. The longer ones along the c axis have pyramidal-coordinated Mn–Mn interatomic bonds with a coordination number of 8 and the shorter ones have planar-coordinated Mn–Mn interatomic bonds with a coordination number of 4. The geometry of the Mn–Mn interatomic bonds in the martensite phase is illustrated on the left side of Fig. 10.

It has been described that the planar-coordinated Mn–Mn bonds show antiferromagnetic exchange coupling while the pyramidal-coordinated Mn–Mn bonds show ferromagnetic exchange coupling.[66,67] The first-order magneto-structural transition arises from the interaction competition between these two different magnetic couplings. As the doping of the smaller atom Co increases, the planar-coordinated antiferromagnetic Mn–Mn bonds shrink while the pyramidal-coordinated ferromagnetic Mn–Mn bonds expand. This strengthens the antiferromagnetic couplings governing by planar-coordinated Mn–Mn bonds and weakens the ferromagnetic couplings governing by pyramidal-coordinated Mn–Mn bonds, which leads to increasing the martensitic transition temperatures.

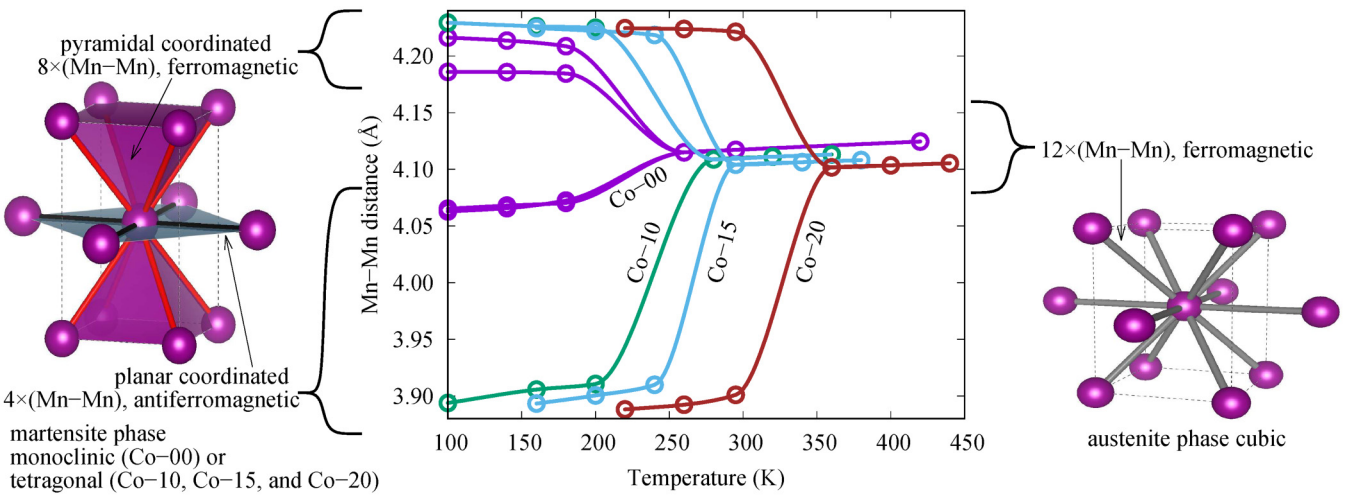

FIG. 10. Temperature dependencies of the Mn–Mn interatomic bonds in $Ni_2Mn_{1-x}Co_xGa$. As the structural transitions occur, a single set of Mn–Mn interatomic bonds present in the austenite $L2_1$ cubic phase splits into two major sets in the low-temperature martensite phase. One set consists of the pyramidal-coordinated Mn–Mn bonds with the longer interatomic distance, a coordination number of 8, and the ferromagnetic coupling, while the other set consists of the planar-coordinated Mn–Mn bonds with the shorter interatomic distance, a coordination number of 4, and the antiferromagnetic coupling.

VI. CONCLUSIONS

To understand the phase transition properties of Co-doped Heusler alloys $Ni_2Mn_{1-x}Co_xGa$ ($0 \leqslant x \leqslant 0.2$), systematic measurements including magnetization, temperature-dependent X-ray diffraction, and calorimetry were conducted. The main findings are summarized as follows: (i) the structural transition temperatures in $Ni_2Mn_{1-x}Co_xGa$ increased with increasing Co concentration x. (ii) As the structural transitions occurs, a single set of Mn–Mn interatomic bonds in the austenite $L2_1$ cubic phase split into two major sets of Mn–Mn interatomic bonds in the low-temperature martensite phase. One set features the pyramidal-coordinated Mn–Mn bonds with the longer interatomic distance, a coordination number of 8, and the ferromagnetic coupling, while the other set exhibits the planar-coordinated Mn–Mn bonds with the shorter interatomic distance, a coordination number of 4, and the antiferromagnetic coupling. (iii) Through direct experimental measurements, a complete phase diagram depicting magnetic and structural transitions up to the melting points was constructed. These findings not only provides the evolution of phase transitions for further fundamental research but also offers valuable insights for practical material design.

ACKNOWLEDGMENTS

S. Stadler acknowledges support from the U.S. Department of Energy, Office of Basic Energy Sciences under Award No. DE-FG02-13ER46946. N. Ali and S. Talapatra acknowledge support from the U.S. Department of Energy, Office of Basic Energy Sciences under Award No. DE-FG02-06ER46291. D. P. Young acknowledges support from the U.S. National Science Foundation, Division of Materials Research under Award No. NSF-DMR-1904636. Xiaojian Bai is supported by the Louisiana Board of Regents under Award No. AM230440. The DSC data used in this work were collected at the Center for Advanced Microstructures and Devices, Louisiana State University under the supervision of A. Roy. This research used resources of the Advanced Photon Source, a U.S. Department of Energy (DOE) Office of Science User Facility operated for the DOE Office of Science by the Argonne National Laboratory under Contract No. DE-AC02-06CH11357.

AUTHOR DECLARATIONS

Conflict of Interest

The authors have no conflicts to disclose.

Author Contributions

Jing-Han Chen: Conceptualization (lead); Data curation (lead); Formal analysis (lead); Investigation (lead); Methodology (lead); Writing – original draft (lead); Writing – review & editing (equal). **Tej Poudel Chhetri:** Methodology (supporting); Writing – review & editing (supporting). **Nathaniel Wrobel:** Methodology (supporting); Writing – review & editing (supporting). **Xiaojian Bai:** Resources (supporting); Writing – review & editing (supporting). **David P. Young:** Resources (supporting); Writing – review & editing (supporting). **Igor Dubenko:** Writing – review & editing (supporting). **Saikat Talapatra:** Writing – review & editing (supporting). **Naushad Ali:** Writing – review & editing (supporting). **Shane Stadler:** Funding acquisition (lead); Resources (lead); Writing – review & editing (lead).

DATA AVAILABILITY

The data that support the findings of this study are available from the corresponding author upon reasonable request.

REFERENCES

[1]F. Heusler, W. Starck, and E. Haupt, "Magnetisch-chemische studien," Verh. Dtsch. Phys. Ges. **5**, 219–232 (1903).
[2]P. J. Webster, K. R. A. Ziebeck, S. L. Town, and M. S. Peak, "Magnetic order and phase transformation in Ni_2MnGa," Philos. Mag. B **49**, 295–310 (1984).
[3]J.-H. Chen, T. Poudel Chhetri, A. T. Grant, C.-K. Chang, D. P. Young, I. Dubenko, N. Ali, and S. Stadler, "The effects of Cu-substitution and high-pressure synthesis on phase transitions in Ni_2MnGa Heusler alloys," J. Alloys Compd. **900**, 163480 (2022).
[4]R. Tickle and R. James, "Magnetic and magnetomechanical properties of Ni_2MnGa," J. Magn. Magn. Mater. **195**, 627–638 (1999).
[5]A. Planes, L. Mañosa, and M. Acet, "Magnetocaloric effect and its relation to shape-memory properties in ferromagnetic Heusler alloys," J. Phys.: Condens. Matter **21**, 233201 (2009).
[6]Y. Sutou, Y. Imano, N. Koeda, T. Omori, R. Kainuma, K. Ishida, and K. Oikawa, "Magnetic and martensitic transformations of NiMnX(X=In,Sn,Sb) ferromagnetic shape memory alloys," Appl. Phys. Lett. **85**, 4358–4360 (2004).
[7]T. Krenke, E. Duman, M. Acet, E. F. Wassermann, X. Moya, L. Mañosa, A. Planes, E. Suard, and B. Ouladdiaf, "Magnetic superelasticity and inverse magnetocaloric effect in Ni-Mn-In," Phys. Rev. B **75**, 104414 (2007).
[8]J.-H. Chen, N. M. Bruno, Z. Ning, W. A. Shelton, I. Karaman, Y. Huang, J. Li, and J. H. Ross, Jr., "Relative cooling power enhancement by tuning magneto-structural stability in Ni-Mn-In Heusler alloys," J. Alloys Compd. **744**, 785–790 (2018).
[9]J.-H. Chen, N. M. Bruno, I. Karaman, Y. Huang, J. Li, and J. H. Ross, Jr., "Calorimetric and magnetic study for $Ni_{50}Mn_{36}In_{14}$ and relative cooling power in paramagnetic inverse magnetocaloric systems," J. Appl. Phys. **116**, 203901 (2014).
[10]J.-H. Chen, N. M. Bruno, I. Karaman, Y. Huang, J. Li, and J. H. Ross, Jr., "Direct measure of giant magnetocaloric entropy contributions in Ni-Mn-In," Acta Mater. **105**, 176–181 (2016).
[11]Y. Huang, Q. Hu, N. Bruno, J.-H. Chen, I. Karaman, J. H. Ross, Jr., and J. Li, "Giant elastocaloric effect in directionally solidified Ni-Mn-In magnetic shape memory alloy," Scr. Mater. **105**, 42–45 (2015).
[12]F. S. Liu, Q. B. Wang, W. Q. Ao, Y. J. Yu, L. C. Pan, and J. Q. Li, "Magnetocaloric effect in high Ni content $Ni_{52}Mn_{48-x}In_x$ alloys under low field change," J. Magn. Magn. Mater. **324**, 514–518 (2012).
[13]N. M. Bruno, C. Yegin, I. Karaman, J.-H. Chen, J. H. Ross, Jr., J. Liu, and J. Li, "The effect of heat treatments on $Ni_{43}Mn_{42}Co_4Sn_{11}$ meta-magnetic shape memory alloys for magnetic refrigeration," Acta Mater. **74**, 66–84 (2014).
[14]N. V. Rama Rao, J. A. Chelvane, V. Chandrasekaran, A. V. Morozkin, J. Lamsal, W. B. Yelon, R. Nirmala, K. G. Suresh, and S. K. Malik, "Neutron diffraction studies on the Heusler alloy $Ni_{50}Mn_{37}Sb_{13}$," J. Appl. Phys. **109**, 07A907 (2011).
[15]C. Zhang, H. Yan, Y. Zhang, C. Esling, X. Zhao, and L. Zuo, "Crystal structure and crystallographic characteristics of martensite in $Ni_{50}Mn_{38}Sb_{12}$ alloys," J. Appl. Crystallogr. **49**, 513–519 (2016).
[16]J. Du, Q. Zheng, W. J. Ren, W. J. Feng, X. G. Liu, and Z. D. Zhang, "Magnetocaloric effect and magnetic-field-induced shape recovery effect at room temperature in ferromagnetic Heusler alloy Ni-Mn-Sb," J. Phys. D: Appl. Phys. **40**, 5523 (2007).

[17]R. Sahoo, A. Das, N. Stuesser, and K. G. Suresh, "Field dependent neutron diffraction study in $Ni_{50}Mn_{38}Sb_{12}$ Heusler alloy," Appl. Phys. Lett. **110**, 021902 (2017).
[18]V. Sánchez-Alarcos, J. Pérez-Landazábal, V. Recarte, I. Lucia, J. Vélez, and J. Rodríguez-Velamazán, "Effect of high-temperature quenching on the magneto-structural transformations and the long-range atomic order of Ni-Mn-Sn and Ni-Mn-Sb metamagnetic shape memory alloys," Acta Mater. **61**, 4676–4682 (2013).
[19]M. Khan, N. Ali, and S. Stadler, "Inverse magnetocaloric effect in ferromagnetic $Ni_{50}Mn_{37+x}Sb_{13-x}$ Heusler alloys," J. Appl. Phys. **101**, 053919 (2007).
[20]T. Krenke, E. Duman, M. Acet, E. F. Wassermann, X. Moya, L. Mañosa, and A. Planes, "Inverse magnetocaloric effect in ferromagnetic Ni-Mn-Sn alloys," Nat. Mater. **4**, 450–454 (2005).
[21]J. Mohd Jani, M. Leary, A. Subic, and M. A. Gibson, "A review of shape memory alloy research, applications and opportunities," Mater. Des. **56**, 1078–1113 (2014).
[22]C. Zimm, A. Jastrab, A. Sternberg, V. K. Pecharsky, K. A. Gschneidner, Jr., M. Osborne, and I. Anderson, *Description and Performance of a Near-Room Temperature Magnetic Refrigerator* (Springer US, Boston, MA, 1998), Vol. 43, pp. 1759–1766.
[23]F. Hames, "Ferromagnetic-alloy phases near the compositions Ni_2MnIn, Ni_2MnGa, Co_2MnGa, Pd_2MnSb, and PdMnSb," J. Appl. Phys. **31**, S370–S371 (1960).
[24]L. Righi, F. Albertini, L. Pareti, A. Paoluzi, and G. Calestani, "Commensurate and incommensurate '5M' modulated crystal structures in Ni-Mn-Ga martensitic phases," Acta Mater. **55**, 5237–5245 (2007).
[25]Z. Li, Y. Zhang, C. Esling, X. Zhao, and L. Zuo, "Twin relationships of 5M modulated martensite in Ni-Mn-Ga alloy," Acta Mater. **59**, 3390–3397 (2011).
[26]L. Righi, F. Albertini, G. Calestani, L. Pareti, A. Paoluzi, C. Ritter, P. A. Algarabel, L. Morellon, and M. Ricardo Ibarra, "Incommensurate modulated structure of the ferromagnetic shape-memory Ni_2MnGa martensite," J. Solid State Chem. **179**, 3525–3533 (2006).
[27]L. Righi, F. Albertini, E. Villa, A. Paoluzi, G. Calestani, V. Chernenko, S. Besseghini, C. Ritter, and F. Passaretti, "Crystal structure of 7M modulated Ni-Mn-Ga martensitic phase," Acta Mater. **56**, 4529–4535 (2008).
[28]R. Overholser, M. Wuttig, and D. Neumann, "Chemical ordering in Ni-Mn-Ga Heusler alloys," Scr. Mater. **40**, 1095–1102 (1999).
[29]H. Ishikawa, R. Umetsu, K. Kobayashi, A. Fujita, R. Kainuma, and K. Ishida, "Atomic ordering and magnetic properties in $Ni_2Mn(Ga_xAl_{1-x})$ Heusler alloys," Acta Mater. **56**, 4789–4797 (2008).
[30]K. Momma and F. Izumi, "*VESTA3* for three-dimensional visualization of crystal, volumetric and morphology data," J. Appl. Crystallogr. **44**, 1272–1276 (2011).
[31]M. A. Uijttewaal, T. Hickel, J. Neugebauer, M. E. Gruner, and P. Entel, "Understanding the phase transitions of the Ni_2MnGa magnetic shape memory system from first principles," Phys. Rev. Lett. **102**, 035702 (2009).
[32]B. Himmetoglu, V. M. Katukuri, and M. Cococcioni, "Origin of magnetic interactions and their influence on the structural properties of Ni_2MnGa and related compounds," J. Phys.: Condens. Matter **24**, 185501 (2012).
[33]Z. H. Liu, M. Zhang, W. Q. Wang, W. H. Wang, J. L. Chen, G. H. Wu, F. B. Meng, H. Y. Liu, B. D. Liu, J. P. Qu, and Y. X. Li, "Magnetic properties and martensitic transformation in quaternary Heusler alloy of NiMnFeGa," J. Appl. Phys. **92**, 5006–5010 (2002).
[34]J. C. Tróchez, J. L. Camargo, I. Piñeres, and D. A. Landínez Tellez, "Effect of Fe on thermal and electrical properties in $Ni_2Mn_{1-x}Fe_xGa$ Heusler alloys," Physica B **558**, 38–43 (2019).
[35]D. Kikuchi, T. Kanomata, Y. Yamaguchi, H. Nishihara, K. Koyama, and K. Watanabe, "Magnetic properties of ferromagnetic shape memory alloys $Ni_2Mn_{1-x}Fe_xGa$," J. Alloys Compd. **383**, 184–188 (2004).
[36]A. Nespoli, C. A. Biffi, E. Villa, and A. Tuissi, "Effect of heating/cooling rate on martensitic transformation of NiMnGa-Co high temperature ferromagnetic shape memory alloys," J. Alloys Compd. **690**, 478–484 (2017).
[37]M. Khan, I. Dubenko, S. Stadler, and N. Ali, "The structural and magnetic properties of $Ni_2Mn_{1-x}M_xGa$ (M = Co, Cu)," J. Appl. Phys. **97**, 10M304 (2005).
[38]M. Khan, S. Stadler, and N. Ali, "Intermartensitic transformations in $Ni_2Mn_{1-x}Co_xGa$ Heusler alloys," J. Appl. Phys. **99**, 08M705 (2006).
[39]A. M. Gomes, M. Khan, S. Stadler, N. Ali, I. Dubenko, A. Y. Takeuchi, and A. P. Guimarães, "Magnetocaloric properties of the $Ni_2Mn_{1-x}(Cu, Co)_xGa$ Heusler alloys," J. Appl. Phys. **99**, 08Q106 (2006).
[40]Y. Adachi, R. Kouta, M. Fujio, T. Kanomata, R. Y. Umetsu, X. Xu, and R. Kainuma, "Magnetic phase diagram of Heusler alloy system $Ni_2Mn_{1-x}Cr_xGa$," Phys. Procedia **75**, 1187–1191 (2015).
[41]M. Khan, J. Brock, and I. Sugerman, "Anomalous transport properties of $Ni_2Mn_{1-x}Cr_xGa$ Heusler alloys at the martensite-austenite phase transition," Phys. Rev. B **93**, 054419 (2016).
[42]T. Sakon, N. Fujimoto, T. Kanomata, and Y. Adachi, "Magnetostriction of $Ni_2Mn_{1-x}Cr_xGa$ Heusler alloys," Metals **7**, 410 (2017).
[43]C. Seguí, J. Torrens-Serra, E. Cesari, and P. Lázpita, "Optimizing the caloric properties of Cu-doped Ni-Mn-Ga alloys," Materials **13**, 419 (2020).
[44]A. Us Saleheen, J.-H. Chen, D. P. Young, I. Dubenko, N. Ali, and S. Stadler, "Critical behavior in Ni_2MnGa and $Ni_2Mn_{0.85}Cu_{0.15}Ga$," J. Appl. Phys. **123**, 203904 (2018).
[45]Z. Li, N. Zou, C. F. Sánchez-Valdés, J. L. S. Llamazares, B. Yang, Y. Hu, Y. Zhang, C. Esling, X. Zhao, and L. Zuo, "Thermal and magnetic field-induced martensitic transformation in $Ni_{50}Mn_{25-x}Ga_{25}Cu_x$ $(0 \leqslant x \leqslant 7)$ melt-spun ribbons," J. Phys. D: Appl. Phys. **49**, 025002 (2016).
[46]S. Stadler, M. Khan, J. Mitchell, N. Ali, A. M. Gomes, I. Dubenko, A. Y. Takeuchi, and A. P. Guimarães, "Magnetocaloric properties of $Ni_2Mn_{1-x}Cu_xGa$," Appl. Phys. Lett. **88**, 192511 (2006).
[47]C. Jiang, J. Wang, P. Li, A. Jia, and H. Xu, "Search for transformation from paramagnetic martensite to ferromagnetic austenite: NiMnGaCu alloys," Appl. Phys. Lett. **95**, 012501 (2009).
[48]J. F. Duan, Y. Long, B. Bao, H. Zhang, R. C. Ye, Y. Q. Chang, F. R. Wan, and G. H. Wu, "Experimental and theoretical investigations of the magnetocaloric effect of $Ni_{2.15}Mn_{0.85-x}Cu_xGa$ $(x = 0.05, 0.07)$ alloys," J. Appl. Phys. **103**, 063911 (2008).
[49]T. Kanomata, K. Endo, N. Kudo, R. Y. Umetsu, H. Nishihara, M. Kataoka, M. Nagasako, R. Kainuma, and K. R. Ziebeck, "Magnetic moment of Cu-modified Ni_2MnGa magnetic shape memory alloys," Metals **3**, 114–122 (2013).
[50]S. Roy, E. Blackburn, S. M. Valvidares, M. R. Fitzsimmons, S. C. Vogel, M. Khan, I. Dubenko, S. Stadler, N. Ali, S. K. Sinha, and J. B. Kortright, "Delocalization and hybridization enhance the magnetocaloric effect in Cu-doped Ni_2MnGa," Phys. Rev. B **79**, 235127 (2009).
[51]U. Devarajan, M. Kannan, R. Thiyagarajan, M. M. Raja, N. V. R. Rao, S. Singh, D. Venkateshwarlu, V. Ganesan, M. Ohashi, and S. Arumugam, "Coupled magnetostructural transition in Ni-Mn-V-Ga Heusler alloys and its effect on the magnetocaloric and transport properties," J. Phys. D: Appl. Phys. **49**, 065001 (2015).
[52]G. Fritsch, V. V. Kokorin, and A. Kempf, "Soft modes in Ni_2MnGa single crystals," J. Phys.: Condens. Matter **6**, L107 (1994).
[53]L. Mañosa, A. Gonzàlez-Comas, E. Obradó, and A. Planes, "Premartensitic phase transformation in the Ni_2MnGa shape memory alloy," Mater. Sci. Eng. A **273-275**, 329–332 (1999).
[54]F. Zuo, X. Su, and K. H. Wu, "Magnetic properties of the premartensitic transition in Ni_2MnGa alloys," Phys. Rev. B **58**, 11127–11130 (1998).
[55]A. H. Morrish, *The Physical Principles of Magnetism* (John Wiley & Sons, Inc., 2001).
[56]B. D. Cullity and C. D. Graham, *Introduction to Magnetic Materials* (John Wiley & Sons, Inc., 2011).
[57]E. Şaşoğlu, L. M. Sandratskii, and P. Bruno, "Pressure dependence of the Curie temperature in Ni_2MnSn Heusler alloy: A first-principles study," Phys. Rev. B **71**, 214412 (2005).

[58]E. Şaşoğlu, L. M. Sandratskii, and P. Bruno, "Role of conduction electrons in mediating exchange interactions in Mn-based Heusler alloys," Phys. Rev. B **77**, 064417 (2008).
[59]E. Şaşoğlu, L. M. Sandratskii, and P. Bruno, "First-principles calculation of the intersublattice exchange interactions and Curie temperatures of the full Heusler alloys Ni_2MnX (X = Ga, In, Sn, Sb)," Phys. Rev. B **70**, 024427 (2004).
[60]K. Shirakawa, T. Kanomata, and T. Kaneko, "Effect of hydrostatic pressure on the Curie temperature of the Heusler alloys Au_2MnAl and Pd_2MnZ (Z = Sn and Sb)," J. Magn. Magn. Mater. **70**, 421–422 (1987).
[61]B. H. Toby and R. B. Von Dreele, "*GSAS-II*: The genesis of a modern open-source all purpose crystallography software package," J. Appl. Crystallogr. **46**, 544–549 (2013).
[62]T. Eto, Y. Nakamoto, T. Kagayama, Y. Adachi, S. Kawaguchi, N. Hirao, Y. Uwatoko, M. Nagasako, and T. Kanomata, "Pressure-induced structural phase transition in the ferromagnetic Heusler alloy Ni_2MnGa," Phys. Rev. B **109**, 014101 (2024).
[63]M. Kataoka, K. Endo, N. Kudo, T. Kanomata, H. Nishihara, T. Shishido, R. Y. Umetsu, M. Nagasako, and R. Kainuma, "Martensitic transition, ferromagnetic transition, and their interplay in the shape memory alloys $Ni_2Mn_{1-x}Cu_xGa$," Phys. Rev. B **82**, 214423 (2010).
[64]C. Kittel, "Model of exchange-inversion magnetization," Phys. Rev. **120**, 335–342 (1960).
[65]C. P. Bean and D. S. Rodbell, "Magnetic disorder as a first-order phase transformation," Phys. Rev. **126**, 104–115 (1962).
[66]V. D. Buchelnikov, V. V. Sokolovskiy, H. C. Herper, H. Ebert, M. E. Gruner, S. V. Taskaev, V. V. Khovaylo, A. Hucht, A. Dannenberg, M. Ogura, H. Akai, M. Acet, and P. Entel, "First-principles and Monte Carlo study of magnetostructural transition and magnetocaloric properties of $Ni_{2+x}Mn_{1-x}Ga$," Phys. Rev. B **81**, 094411 (2010).
[67]I. Galanakis and E. Şaşoğlu, "Variation of the magnetic properties of Ni_2MnGa Heusler alloy upon tetragonalization: A first-principles study," J. Phys. D: Appl. Phys. **44**, 235001 (2011).